POLITEHNICA University of Bucharest

Ph.D Thesis

Theoretical and experimental contribution for steady of the hermetic reciprocating compressor and hot wall condenser in the small household refrigerator using R600a, R1234yf, and R134a.

By

Saleh Jassim Saleh AL-QAISY

A thesis submitted in partial fulfillment of the requirements for the degree of Doctor of Philosophy in Mechanical Engineering, University POLITEHNICA of

Bucharest, Romania

Supervised by
Prof. Dr. Eng. Viorel BADESCU

Romania, Bucharest, 2023

Contents

1 Introduction

1.1 Background

Electric energy is the basis on which the humans of the planet depend for the development of their standard of living as the increase in development in life requires causes an increase in the electrical energy consumption, Bista *et al* [1]. The increase in energy consumption, Douri *et al* [2] which increases carbon dioxide emissions, which is a major concern, is causing climate change. Household refrigerator (HR) play a significant role in all phases of a primary load of daily electrical operations in homes and buildings. Where HR consumes about 6% of the electricity generated around the world. Figure 1-1 show the power consumption in some countries Choi *et al* [3] and Bista *et al* [1].
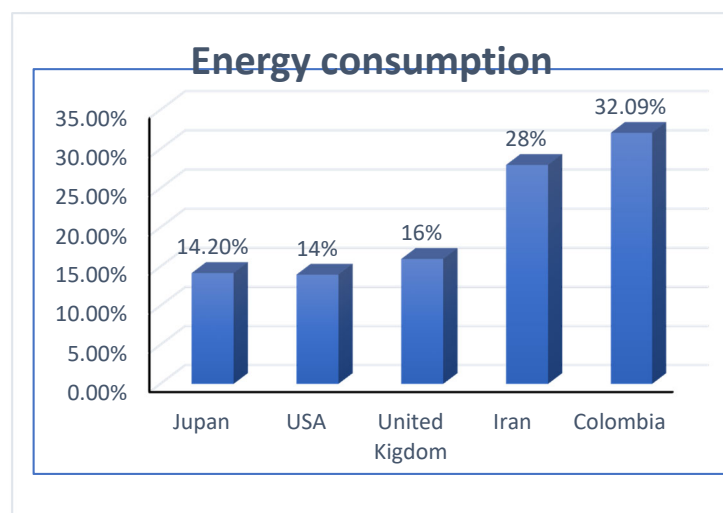
Figure 1-1: power consumption by the household refrigerator for some countries.

To improve Vapour Compression Refrigeration System (VCRs) efficiency, compression and expansion losses must be reduced, especially heat exchangers, compressors and expansion tools. Click or tap here to enter text..In general, a HR's operating principle is based on a VCRs, and Suction Line Heat Exchanger (SLHX). Usually, Refrigerants used in VCRs have negligible to no impact on GWP. One of the refrigerants currently in use is R600a. The R134a refrigerant is considered to be replaced by the R600a. Previously used which has been prohibited due to its major effect on the GWP despite its high efficiency. However, due to its flammability, the R600a cannot be considered an ideal refrigerant, Choi *et al* [3].The various refrigeration requirements that impact the performance will be discussed in chapter two. Researchers, however, intensify efforts to boost the effectiveness and performance of environmentally friendly refrigeration systems.

1.2 Refrigeration Systems

1.2.1 Vapour Compression Refrigeration Systems

One of the most common appliances for refrigeration systems is VCRS, which is operated with many different types of HRs, Choi *et al*.[3], Douri *et al* [7].The SLHX system is used by many HRs today to improve the performance. The SLHX system works to transfer heat between the capillary tube and the evaporator, to increase the area of liquid (sub-cooling) and increase the temperature of the vapour entering the compressor (sub-heating).
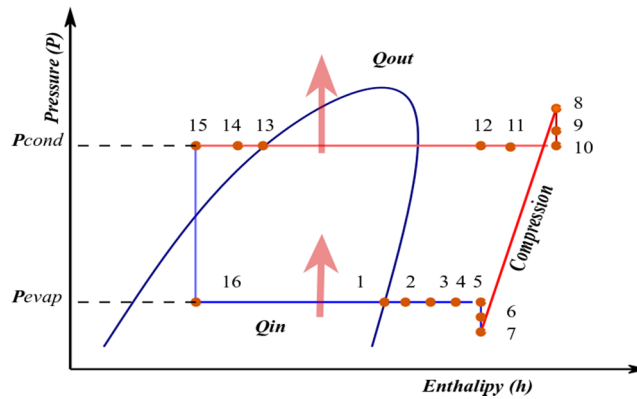
Figure 1-2 The real vapour compression cycle

There are sixteen important processes that suggest the thermodynamic analysis that to be observed in p-h diagram of figure 1.2, Navarro *et al.* [8] and Ramesha [9].

1.2.1.1 Compression process

1.2.1.2 Condensation process

1.2.1.3 Throttle and expansion process

1.2.1.4 Evaporation process

1.2.2 Main Components of Refrigeration System

Refrigeration systems composed of multiple parts, including compressor, condenser, expansion or throttling device, evaporator and refrigerant are considered the main components of the system, figure 1.3.
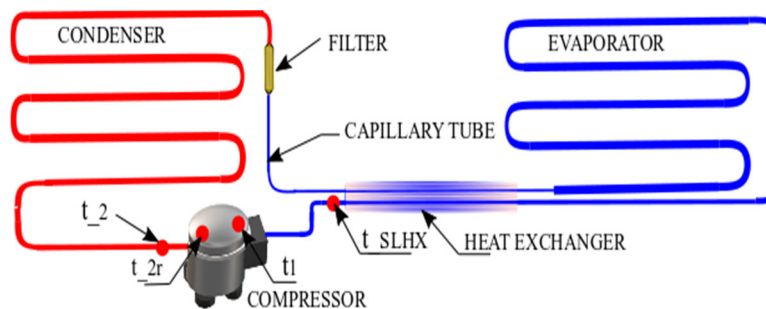
Figure 1-3: Main components of refrigerant system

1.2.2.1 Compressors

1.2.2.1.1 Reciprocating Compressor

In general, the piston moves inside a cylinder with reciprocal and constant motion between two points; the top dead centre (TDC), where the clearance volume is the smallest possible. The bottom dead centre (BDC) is where the volume is the largest possible size. Stroke is the name given to the separation between the two points., ÇENGEL [10]. The diameter is called a Bore. The process of extracting the refrigerant is carried out through the inlet or suction valve, and the refrigerant is compressed and exits the cylinder through the outlet or discharge valve.

 In Figure 1.4, 1.5, the refrigerant experiences two types of pressure drop when entering the cylinder, as the first pressure drop P_2 often occurs when the suction valve is sucked to move to P_3, and then the second pressure drop in the discharge valve occurs when the refrigerant discharge moves from P_4 to P_5, Pe´rez-Segarra *et al.* [11] Ndiaye and Bernier [12].
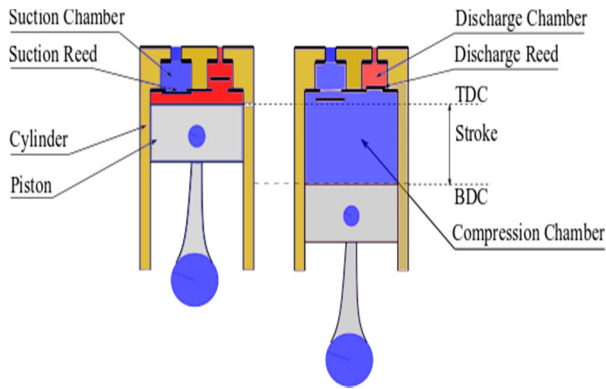
Figure 1-4: Recip. compressor piston   Figure 1-5: Indicator diagram of compressor
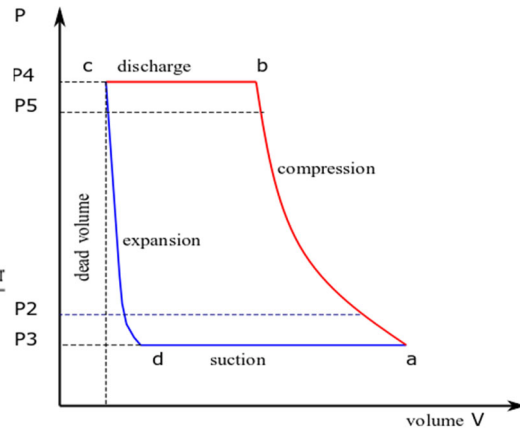
1.2.2.1.2 Hermetic Reciprocating Compressors

Hermetic compressors are often used in small applications, including in the HR, Ibrahim Dincer [13]. Figure 1.6. represent the internal parts of HRC.
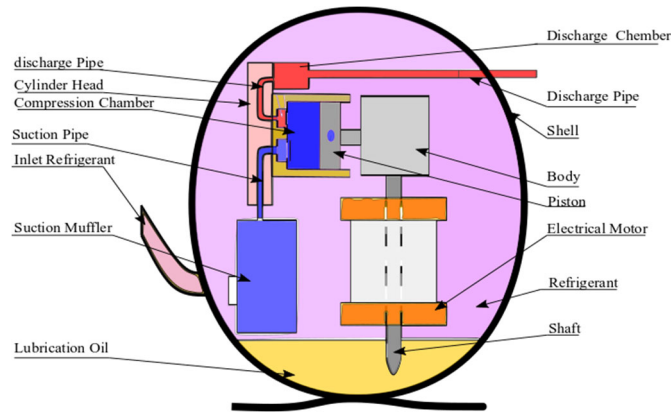
Figure 1-6: Hermetic reciprocating compressor

1.2.2.2 Condenser

1.2.2.3 Expansion and throttling device

1.2.2.4 Evaporator

1.2.3 Refrigerants

Refrigerants are the operating medium used within the refrigeration and air conditioning systems, and in the mode of latent or sensitive heat, it can transport and dissipate heat, which are more efficient with sufficient properties to get from liquid to gas, and vice versa.

1.2.3.1 Refrigerant thermodynamic properties

1.2.3.2 Refrigerant numbering

1.2.3.3 Safety requirements

1.2.4 Lubrication oil

1.3 Problem Statement

There are three fundamental reasons that made all researchers work to enhance the effectiveness of refrigeration systems, especially the HR, as in figure 1.7.
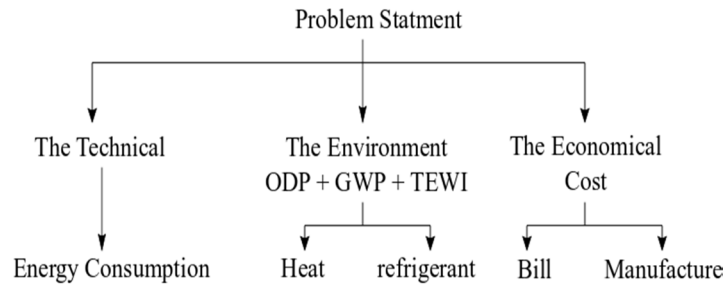
Figure 1-7 Problem Statement

1.3.1 Environmental Effect

1.3.2 The Technical Effect

1.3.3 Economical Cost

1.4 Aim of the Thesis

The main aims of the thesis are synthesized below:

- To study the operation of HRC found on small household refrigerators (HR), for different ambient temperatures using refrigerants R600a, R134a, and R1234yf.

- To study the operation of HWC found on small HR, for different ambient temperatures using refrigerants R600a, R134a, and R1234yf.

- To validate the theoretical results using data from an experimental setup based on a small HR.

2   Literature Review Regarding Compressor and Condenser

Due to the development of human life. Refrigerating systems, such as refrigerators as well as air conditioners have become required throughout every house, as the energy consumption of these systems reached 32-50 % of all energy consumption in residences, Gürel *et al* [14] and Jin *et al* [15]. The mechanical theory of compression applied to VCRS depending on the heat is absorbed from the refrigerant from the material to be cooled, and this absorbed heat is to be rejected by condensation to the outside, Faraji [16]. Generally, refrigerators are using VCRS which includes a compressor worked as the system heart, condenser as a heat expeller, capillary tube as a throttle, and the evaporator as the heat absorber, Bansal [17].

2.1   Compressor

2.1.1   Hermetic Reciprocating Compressor Operation parameters

Figure (2.1) indicates the areas where the direct heat transfer occurs to the refrigerant and lubricating oil used and then to the compressor shell.
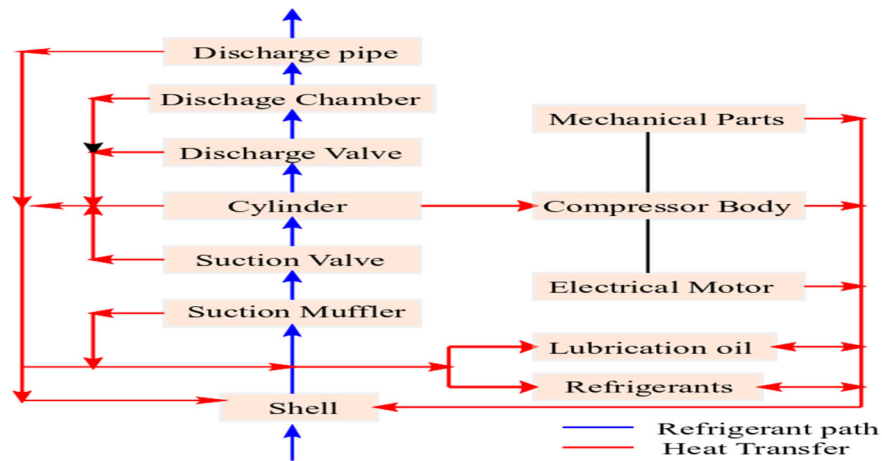
Figure 2-1: Heat transfer inside the compressor

2.1.1.1   Energy consumption

One of the major aspects on which all researchers and designers operate is to develop a method that reduces energy consumption in air conditioning units, including HR.

In this section, it is possible to follow the factors affecting the energy consumption of the HRC from the literature as evinced in the figure 2.2.
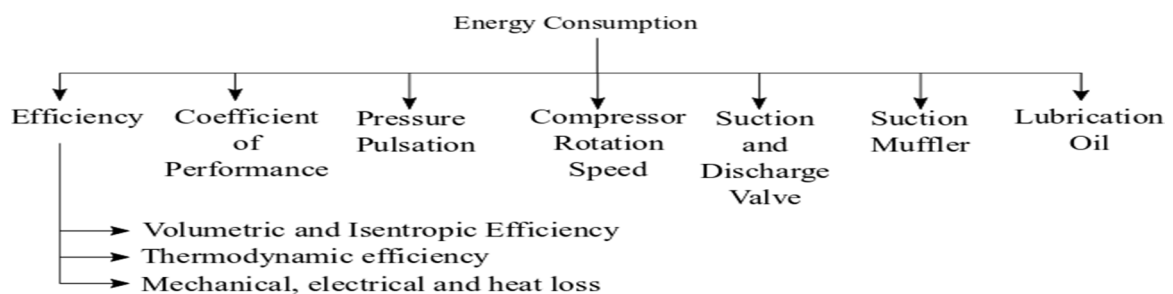
Figure 2-2: Factors affecting the energy consumption

2.1.1.1.1 Efficiency

2.1.1.1.1.1 Volumetric and Isentropic Efficiency

2.1.1.1.1.2 Thermodynamic efficiency

2.1.1.1.1.3 Mechanical, electrical and heat losses efficiencies

2.1.1.1.2 Coefficient of Performance

The ratio between the cooling or heating effect on the net energy input or the work done by the electrical engine is defined as the coefficient of performance, Pe´rez-Segarra *et al.* [11]. The refrigeration system performance depends heavily on the compressor performance and working parameter conditions, Zhou *et al.* [18]. Because of the increasing significance of energy efficiency, compressor performance studies contribute significantly in reducing the overall refrigeration energy consumption, Ozdemir *et al.* [19].

2.1.1.1.3 Pressure pulsation

2.1.1.1.4 Compressor rotational speed

2.1.1.1.5 Suction and discharge valve

Reed valves are usually used throughout, HRC Fig. 2.3,
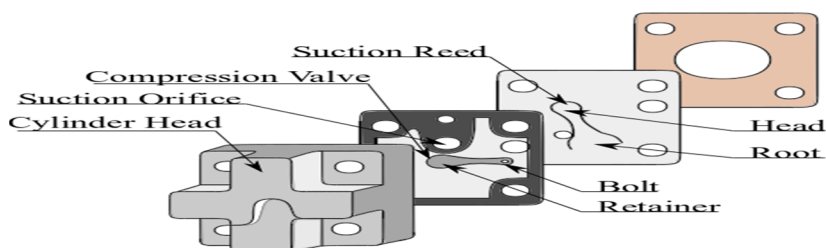
Figure 2-3: Schematic of cylinder head suction and discharge valves

2.1.1.1.6 Suction muffler

2.1.1.1.7 Lubrication oil

Oil lubricant used in the refrigeration system reduces the friction level, noise and cools the refrigerant by transfer heat from the compressors inside the shell, Fig. 2.4.
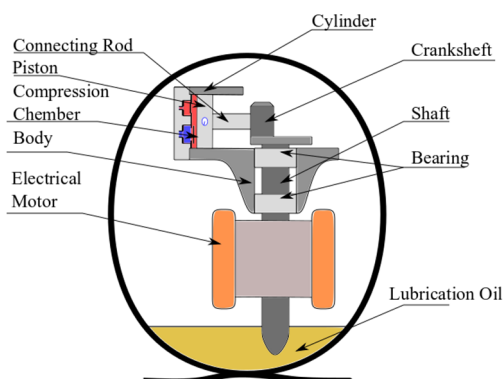
Figure 2-4: Lubrication oil systems in the HRC

2.2 Condenser

HR condensers can be divided into: HWC, wire and tube or natural draft condenser, air-cool condenser, and Micro-channel condenser,

2.2.1 Hot wall condenser

2.2.2 Wire-and-tube condenser

2.2.3 Air-cooled condenser

2.2.4 Micro-channel condenser

3 Experiment Setup Description

3.1 Experimental Setup

Figure 3.1 represents the connecting of experiment main components used in this research. The experiments were conducted using a commercial HRC, running with R600a, designed for HR.
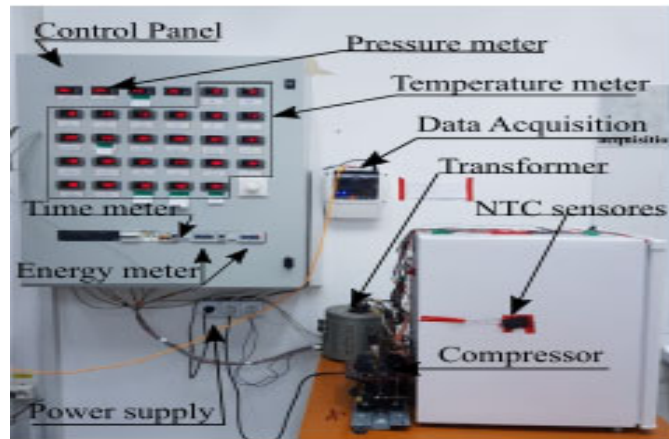
Figure 3-1: System configuration

3.2 The Experiment Components

3.2.1 Small-scale refrigerator
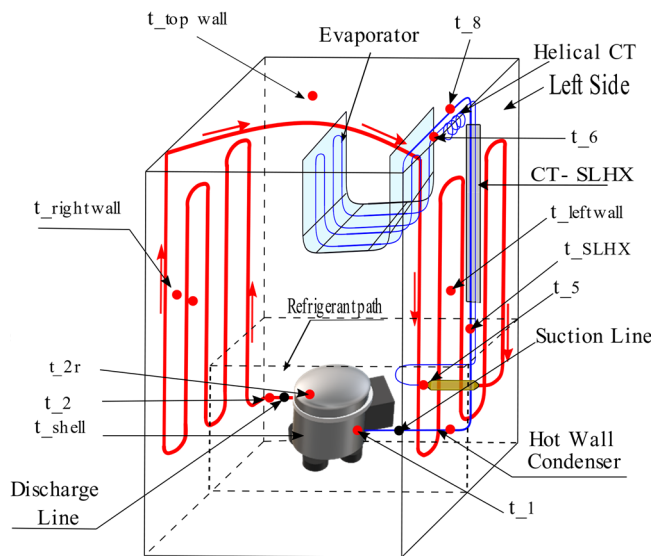
Figure 3-2: NTC sensors position

Figure 3.2 represents the refrigerator used in the location and the distribution of the NTC sensors.

3.3   Experimental Procedures

For the experimental setup of the HRC and refrigerant replacement the following steps were done. An electric cutting machine was used carefully to cut the shell of the HRC type SZ55C1J, which has been used in the experiment. The internal components of the compressor (electric motor, electrical connection point, mechanical motor, and refrigerant discharge tube connection point) have been removed to prevent damage, figure 3.3.

Figure 3-3: Internal component of the experimental compressor

1. For making a ring around the edge of the compressor's upper and lower shell, a rectangular plate of iron measuring 17 cm width and 40 cm long with a thickness of 5 mm was used. The plate of iron was divided into two parts (17cm and 20 cm). The ring's thickness of 5 mm was utilized to prevent denting and distortion during welding the ring over the shell.
2. Before welding, the two rings were smoothed and cleaned to suit the top and lower measurement outer shells of the compressor, after which they were welded to the compressor body, the two shell sections and the rings were cleaned and smoothed again. On the two rings, 22 holes of 6 mm diameter were drilled with an electric drill.
3. The cover of the high-pressure discharge chamber was removed from the discharge chamber, and a 2 mm circular hole was drilled for the installation of an NTC-type thermistor to monitor the refrigerant exiting temperature from the compressor discharge chamber, figure 3.4.

Figure 3-4: Discharge chamber cover

4. An electric drill was used to drill 2 holes, 4 mm diameter. The first hole is near the suction pipe, and the second is on the other side of the lower section of the compressor shell. The compressor contains four NTC sensors installed inside the shell, figure.3.5.
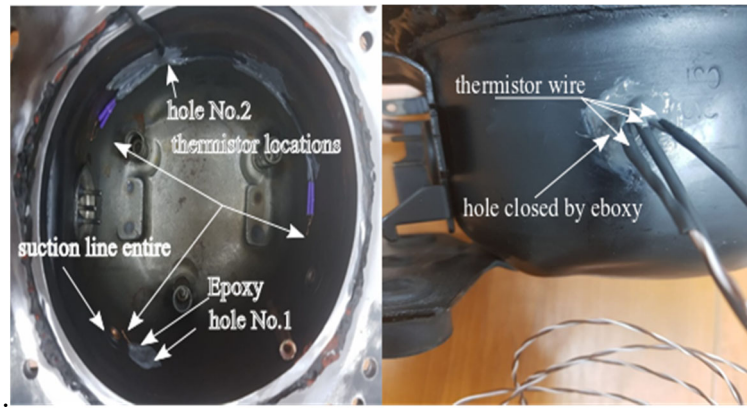
Figure 3-5: Thermistors location inside compressor shell

4 Mathematical Model of HRC and Validation

4.1 Introduction

In this section, the thermodynamic analysis can be used in p-h of figure 4.1; utilizing six essential processes from point 1 to point 5. The following processes have been identified:
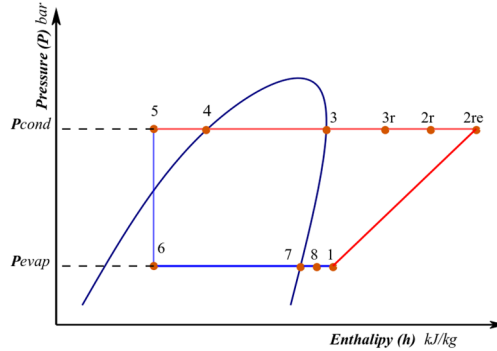
Figure 4-1: Real vapour compression cycle

The figure 4.1 shows the usage of 10-point scale for thermodynamic analysis which is match to the criteria listed below.

4.2 Refrigerant (R600a), (R134a) and (R1234yf) Properties

Refrigerant R600 and R1234yf are used as a replacement for refrigerant R134a.

Table 4-1: properties of the R600a, R134a, R1234yf

Properties	R600a [20],[21], [22], [23], [24]	R134a [25], [26], [27], [28], [29]	R1234yf [22], [25], [26], [27], [30]
numerical designation	Isobutane Methyl-propane	Tetrafluoroethane HydrofluorocarbonH FC134a	Tetrafluoropropen Hydrofluoroolefin HFOs-1234yf
chemical formula	$CH(CH_3)_2CH_3$	CF_3CH_2F	$C_3F_4H_2$
Boiling point at atm.	(-13)-(-9) °C	-26.3°C	-29.4°C
Critical Temperature	134.7°C , 407.81 K	101.1°C , 374.21 K	94.7°C , 367.85 K
Critical pressure [MPa]	3.65	4.06	3.38

4.3 Description of the HRC in Literature Review

4.4 Compressor Mathematical Model

A model is a mathematical representation of a process, usually represented in mathematical equations, to find $\dot{m}$ into compressor by using dimensional and functional parameter can be calculated from the expression, Hu *et al* [31],Hmood *et al* [32], Pop *et al* [33]:

$$\dot{m} = \frac{V_1}{v_1} = \frac{V_2}{v_2} \qquad (1)$$

Compressor real volume flow rate $_{V_1}$ is found by using Pop *et al* [33]:

$$\dot{V_1} = \lambda \cdot \frac{\pi \cdot D^2}{4} \cdot S \cdot \frac{n_r}{60} \cdot i \cdot z \tag{2}$$

Polytropic process can be used to find the volumetric efficiency, Li [34]. For that, the coefficient of volume flow reduction λ [-] can be found from:

$$\lambda_0 = 1 - \varepsilon_0 \cdot \left(H_c^{1/n} - 1 \right) \tag{3}$$

$$\varepsilon_0 = \frac{v_{cl}}{v_{sp}} \tag{4}$$

$$H_c = \frac{p_c}{p_e} \tag{5}$$

The rate of work on vapour in the compression cylinders determined:

$$P_{ex} = \dot{m} \quad \left(h_{2r} - h_{1'} \right) \tag{6}$$

$$P = \frac{\dot{E}_{Comp}^{final} - \dot{E}_{Comp.}^{initial}}{\tau_{operation}^{final} - \tau_{operation}^{initial}} \tag{7}$$

4.5 Dimensional and Functional Parameter of the Compressor

The stability diagram is for working, while the operation is shown in figure 4.2.
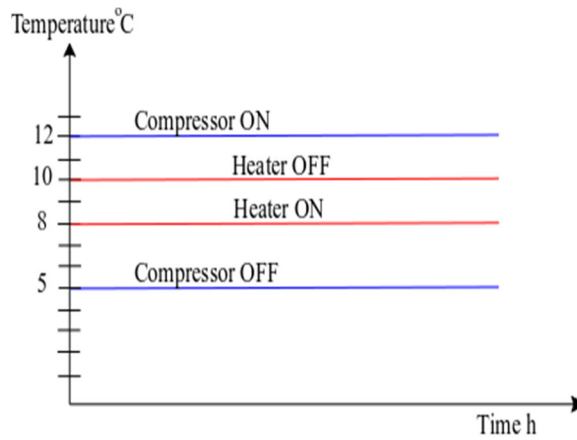
Figure 4-2: Steady-state duration experiments time

The tables below provide details have been measured from the experiments at various ambient temperatures at steady-state condition.

Table 4-2: Experimental for R600a input data [188].

Input parameter	Test 1	Test 2	Test 3	Test 4	Test 5	Test 7	Test 6	Test 8
p_{cond} [bar]	7.17900	7.50557	7.43783	7.59637	7.76803	7.64570	7.82753	7.79338
p_{evap} [bar]	0.51352	0.53246	0.53883	0.53321	0.56016	0.5135	0.55082	0.51387
$t_{\_amb}$ [°C]	22	23	24	25	26	27	28	29
$t_{\_2}$ [°C]	87.83	88.79	89.90	90.39	90.32	92.18	92.72	95.33

t_{2r} [ºC]	59.79	60.58	61.80	62.5	62.97	63.82	64.90	66.35
t_{3r} [ºC]	52.50	54.77	55.85	56.35	56.95	57.58	58.41	59.4
t_1 [ºC]	50.52	51.80	52.97	53.71	53.73	55.98	56.73	59.68
t_{shell} [ºC]	58.28	59.10	59.98	60.82	60.58	62.72	62.92	64.88
t_5 [ºC]	38.87	40.92	41.9	42.75	43.73	43.46	44.45	44.22
T_6[ºC]	-28.52	-29.23	-28.9	-28.32	-28.03	-28.3	-29.28	-28.95
T_8[ºC]	-25.63	-26.81	-26.49	-25.95	-25.63	-27.12	-25.94	-26.71
t_{SLHX} [ºC]	5.69	6.95	9.66	10.95	11.38	12.21	12.46	14.61

4.6   Validation of the Mathematical Model

The goal for this work is to compute the values of the $\dot{m}$ using the vapour pressure refrigeration system represented by the household refrigeration system. The problem is that the refrigerator works with the R600a, for the purpose of calibrating the work efficiency of the MM that was used. The used refrigerant was compared with other refrigerants, such as R134a and R1234yf, and this will be done by using the same refrigeration system to study the practical and theoretical convergence of these refrigerants.

4.7   Results

The figures below represent all the properties and the results obtained from the experiments have been taken for several data.

Figure 4.3 we can observe that when the ambient temperature increases, the temperature of the refrigerant in the muffler discharge also increases.
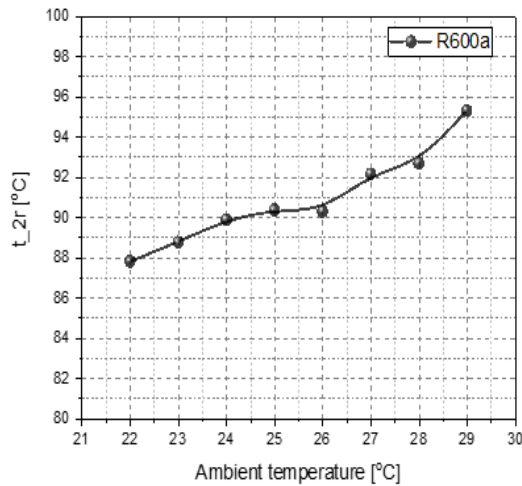
Figure 4-3: R600a ambient and muffler discharge temperature.

Figure 4.4 displays the discharge temperature. When selecting an alternative, the discharge temperature is a crucial factor to take into account.

The discharge temperature was effected by oils and compressor parts stability.

The discharge temperature is increasing with the ambient temperatures, as shown in figure 4.5.
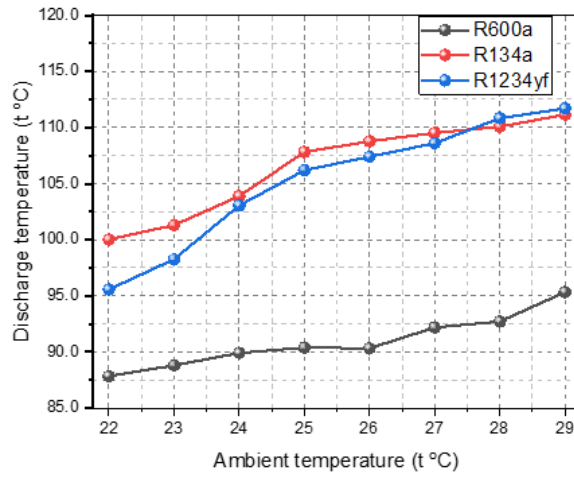
Figure 4-4: Discharge and ambient temperature.

Figure 4.5 presents the effect of ambient temp. on the refrigerant ṁ for the R600a, R134a, and R1234yf ṁ used in the following study. The observed ṁ behavior for R600a, R134a, and R1234yf refrigerants used in this study under the same circumstances was compared at varying ambient temperatures between 22 and 29°C.

Figure 4.6 indicates that the refrigerant used in the systems is affected by ambient temperature, and the compressor power has been measured. One can observe that the R1234yf has the highest power measured, while R134a and R600a have the lowest, respectively.

Figure 4.7 represent the ambient influence to the suction port temperature distribution at the inlet suction with the R600a, R134a, and R1234yf refrigerants. The temperature at the inlet suction of the compressor behaves roughly the same for all refrigerants used in this experiment.
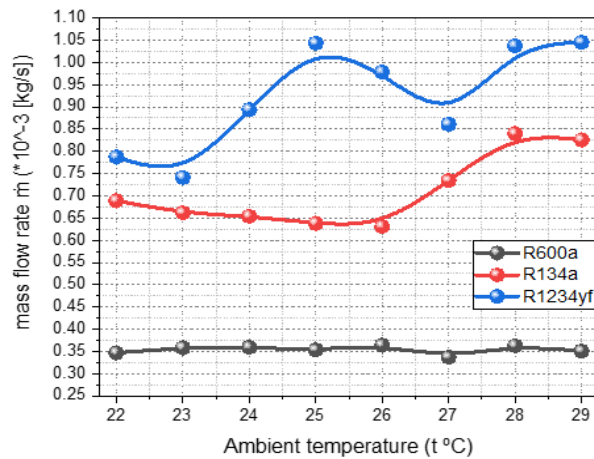
Figure 4-5: Ambient temperature and mass flow rate.
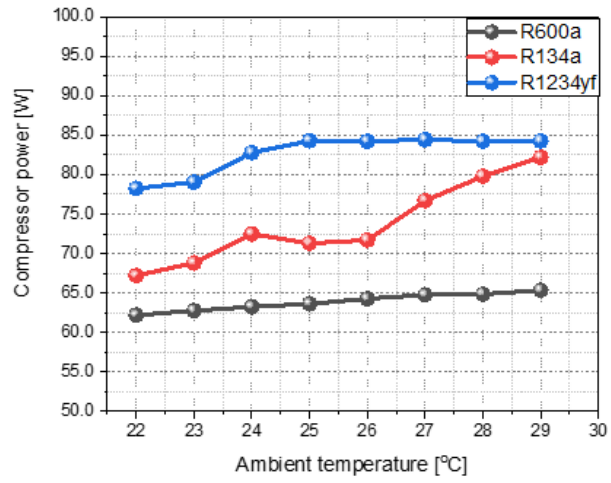
Figure 4-6: Relation between compressor power and ambient temperature
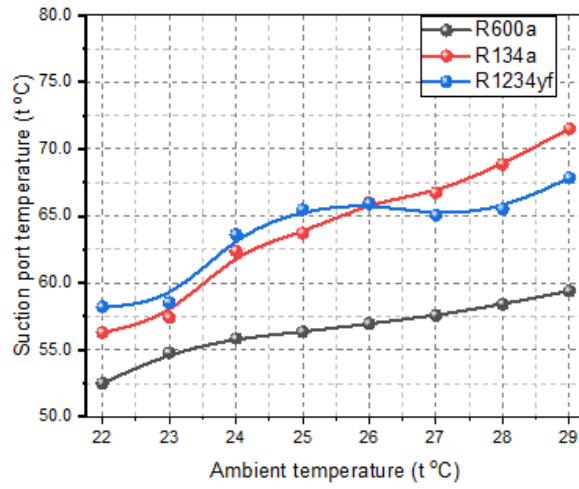
Figure 4-7: Relation between ambient and suction port temperature

5 Mathematical Model of HWC and Validation

5.1 Introduction

The condenser in a refrigeration system is responsible for heat rejection to the environment, Rebora [35]. Figure 5-1

While the number of HR using HWC has increased in recent years, one may observe that there are not many of articles and researches related to this topic.

5.2 HWC Mathematical Model

The overall length [m] estimated from the EES software presented in figure 5.4 will be compared to the original length measured from the refrigerator to validate the MM. In the EES program, the following input data were collected experimentally in the lab.
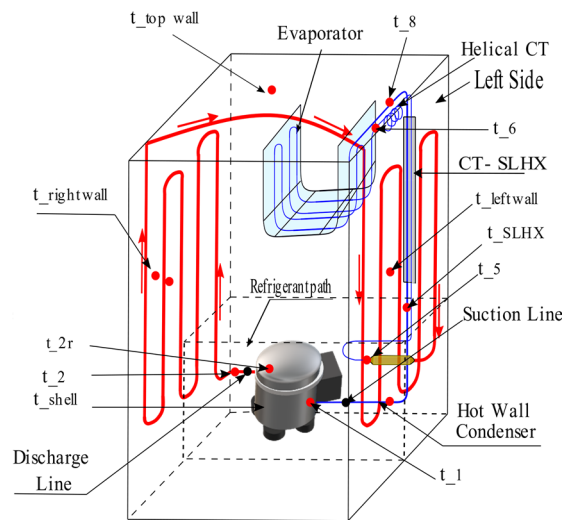
Figure 5-1: HWC in small refrigerator

5.3 Heat Transfer Rate inside Condenser Pipe

The refrigerant with three variable characteristic phases passes inside the condenser, Hermes et al [36], as in figure 5.2

5.3.1 De-super-heating region mathematical model

The super-heating region of HWC can be divided by two sections.

- First section

  The first section starts from the exit point of the compressor (2r) to the entry point to the refrigerator wall (3r), where this a region is directly exposed to the external environment.

- Second section

  This section starts from the entry point to the refrigerator wall (3r) until the saturation point (3), as this region is characterized by not being directly exposed to the external environment. The condenser pipe surface touches the refrigerator wall outer surface on one direction and the thermal insulation on the other direction, figure 5.3.
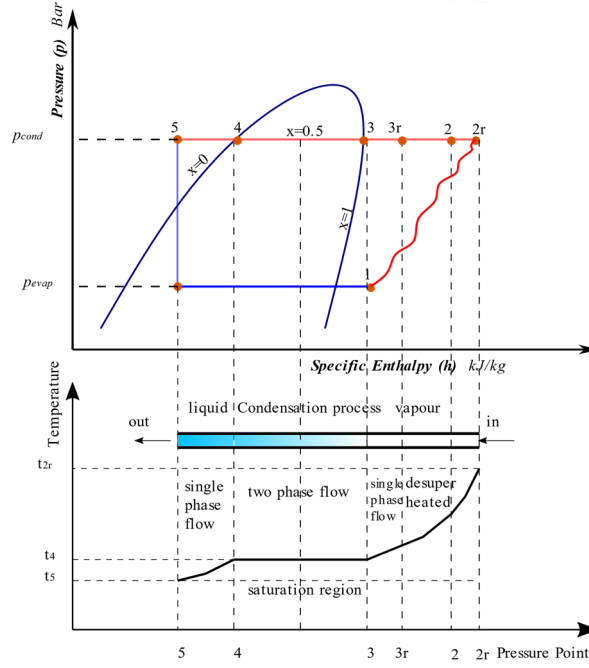
Figure 5-2: Refrigerant thermodynamic processes between HRC and the HWC outlet.
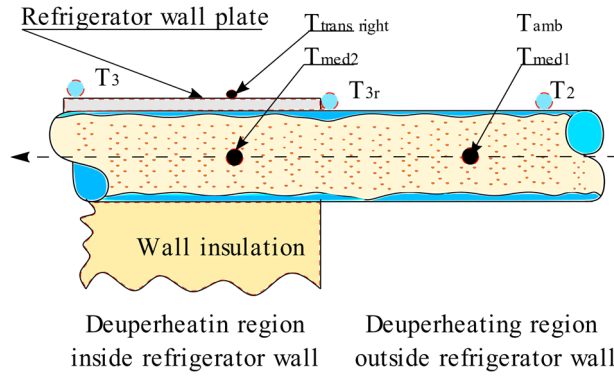
Figure 5-3: De-superheating section.

5.3.1.1 De-super-heated region outside refrigerator wall

In a single-phase region from outside compressor (2) to the point entering refrigerator wall at point (3r), ($\dot{Q}_{d,sh1}$) de-super-heating concentrations can be determined as shown:

$$\dot{Q}_{d,sh1} = \alpha_{sh1} \cdot A_{sh1} \cdot \left(T_{med\,1} - T_{amb} \right) \tag{8}$$

$$A_{sh1} = 3.14 \cdot d_{in} \cdot L_{sh1} \tag{9}$$

Where, (α_{sh1}) represents the convection heat transfer *[W/(m². K)]* at the HWC entering (2), (A_{sh1}) is the surface area *[m²]* between points (2) and (3r), (T_{amb})is the ambient temperature *[K]*, and the medium temperature (T_{med}) the *[K]* could found from:

$$T_{med,1} = \frac{h_2 - h_{3r}}{s_2 - s_{3r}} \tag{10}$$

The Dittus-Boelter equation specifies the turbulent flow coefficients of ($\dot{Q}_{d,sh1}$) in single-phase at the super-heating region, Incropera and De Witt [37] and Gupta and Ram Gopal [38] as:

$$\alpha_{sh1} = 0.023 \cdot Re_2^{0.8} \cdot Pr_2^{0.3} \cdot \frac{k_2}{d_{in}} \tag{11}$$

$$Re_2 = \frac{\rho_2 \cdot u \cdot d_{in.}}{\mu_2} \tag{12}$$

Where, (ρ_2) is the refrigerant density at the outer point of compressor $[kg/m^3]$, (u) is thee mean velocity of the liquid $[m/s]$, and (μ_2) is the dynamic viscosity $[kg/(m\ s)]$, (d_{in}) inside diameter of the pipeline $[m]$.

$$u = \frac{\dot{m}}{\rho_2 \cdot A_{pipe,in}} \tag{13}$$

$$A_{pipe,in} = \frac{\pi \cdot d_{in}^2}{4} \tag{14}$$

Prandtl number (Pr_2) [-] can be found at constant pressure and (T_2).

Where, Reynolds no. is less than 2300 for a certain flow in a circular smooth wall tube, the flow shall be laminar, and it will be turbulent if it is more than 2300, Borremans [39].

5.3.1.2 De-super-heated region inside refrigerator wall

The second section in a single-phase region starts from the point entering the refrigerator wall at point (3r) to the point (3) at the super-heated saturation line. ($\dot{Q}_{d,sh2}$) de-super-heating is determined as:

$$\dot{Q}_{d,sh2} = \alpha_{sh2} \cdot A_{sh2} \cdot \left(T_{med2} - T_{trans,right} \right) \tag{15}$$

(A_{sh2}) is the surface area $[m^2]$ between points (3r) and (3). The region takes into consideration the contact angle (θ) in figure 2-4 between the condenser pipe and the refrigerator wall surface region.

$$A_{sh2} = 3.14 \cdot d_{in} \cdot L_{sh2} \cdot \frac{\theta}{360} \tag{16}$$

The medium temperature (T_{med2}) $[K]$ is found from:

$$T_{med2} = \frac{h_{3r} - h_3}{s_{3r} - s_3} \tag{17}$$

$$L_{sh} = L_{sh,1} + L_{sh,2} \tag{18}$$

5.3.2 Two-Phase Mathematical Model

The main purpose of this work's MM is to predict the HWC thermal performance according to the geometry, which was influenced by the R600a refrigerant flow direction change.
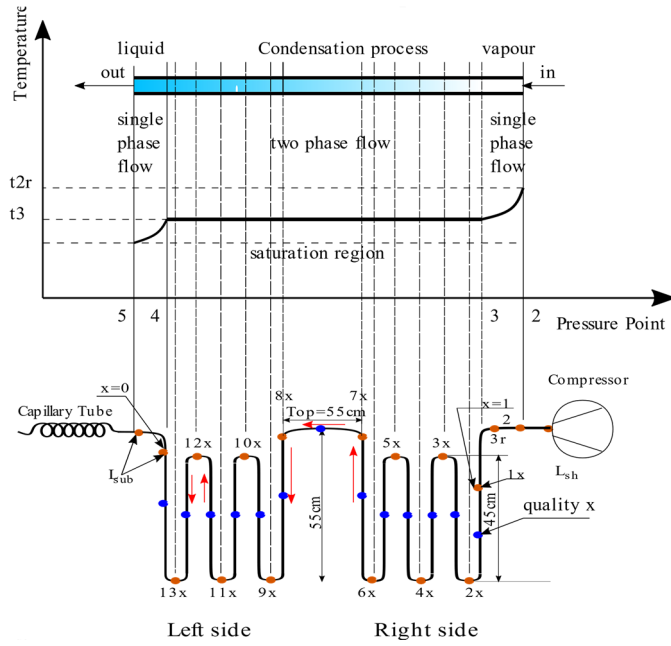
Figure 5-4: Schematic HWC cells diagram.

Following formula can describe the heat transfer throughout two-phase region:

$$\dot{Q}_{tp} = \alpha_{tp} \cdot A_{tp} \cdot \left(T_{med} - T_{trans} \right) \tag{19}$$

5.3.2.1 Two-phase vertical pipe region

For each direction, a separate quality value was calculated. After measuring the average of the enthalpy entering and exiting each cell, the x-quality point was calculated.

In addition to the equation for energy conservation,

$$h_{xn} = \frac{h_{nx} + h_{(n+1)x}}{2} \tag{20}$$

5.3.2.1.1 Down flow path

Convective heat transfer coefficient relationship can be provided by Reynolds numbers with the downward vapour flow, Bansal and Chin [40], Hmood [41].

$$\alpha_{tp,down,(n+1)x} = 0.023 \cdot Re_{l,(n+1)x}^{1/4} \cdot \left[\frac{\rho_l \cdot (\rho_l - \rho_v) g}{\mu_{(n+1)x}^2} \right]^{1/3} \tag{21}$$

$$\mu_{(n+1)x} = \mu_l - \left(x_1 \cdot \left(\mu_l - \mu_v \right) \right) \tag{22}$$

$$K_{(n+1)x} = K_l - \left(x_1 \cdot \left(K_l - K_v \right) \right) \tag{23}$$

$$Re_{l,(n+1)x} = \frac{G_{flux} \cdot (1 - x_1) \cdot d_i}{\mu_l} \tag{24}$$

$$G_{flux} = \frac{\dot{m}}{A_{pipein}} \tag{25}$$

5.3.2.1.2 Upper flow path

The second path in a right-side region starts from the end point of the path one at the bottom of the pipe line (2x). The R600a refrigerant is passing though the upper pipe till reaching the point (3x) which is the end of the cell (2) at the top of the second line. The values have been taken from point (2x) to the point (3x), figure 1.6. ($\dot{Q}_{tp,up,right,2x}$) two-phase upper flow on the right side is determined at n=1 as:

$$\dot{Q}_{tp,up,right,(n+1)x} = \alpha_{tp,vert,up,right,(n+1)x} \cdot A_{(n+1)x} \cdot \left(T_3 - T_{trans,righ} \right) \tag{26}$$

$$\dot{Q}_{tp,up,right,(n+1)x} = \dot{m} \cdot \left(h_{2x} - h_{3x} \right) \tag{27}$$

$$h_{tp,vert,up,right,2x} = 1.47 \cdot K_{2x} \cdot \left[\frac{\rho_l (\rho_l - \rho_v) \cdot g}{\mu_{2x}^2 \cdot Re_{l,2x}} \right]^{1/3} \tag{28}$$

5.3.2.2 Horizontal region mathematical model inside the pipe
The Wallis's correlation for flooding is:

$$j_g = \frac{G_{flux}}{\sqrt{\rho_v \cdot (\rho_l - \rho_v) \cdot d_{in} \cdot g_{gravity}}} \cdot \left(\frac{K_p}{X_{tt}^{1.111} - K_p} \right) \tag{29}$$

$$K_p = \left(\frac{\rho_v}{\rho_l} \right)^{0.555} \cdot \left(\frac{\mu_l}{\mu_v} \right)^{0.111} \tag{30}$$

Lockhart - Martinelli's [42] parameter for turbulent–turbulent flow conditions, Sarma *et al.* [43] is:

$$X_{tt} = \left(\frac{1 - (n+1) \cdot x}{(1+n) \cdot x} \right)^{0.9} \cdot \left(\frac{\rho_v}{\rho_l} \right)^{0.5} \cdot \left(\frac{\mu_l}{\mu_v} \right)^{0.1} \tag{31}$$

$$\dot{Q}_{tp,ann} = \alpha_{tp,ann} \cdot A_{top,ann} \cdot \left(T_3 - T_{trans,top} \right) \tag{32}$$

$$\alpha_{tp,ann} = 0.05 \cdot Re_{ref}^{0.8} \cdot Pr_l^{0.33} \cdot \left(\frac{k_l}{d_{in}} \right) \tag{33}$$

$$Re_{ref} = Re_v \cdot \left(\frac{\mu_v}{\mu_l} \right) \cdot \left(\frac{\rho_l}{\rho_v} \right)^{0.5} + Re_l \tag{34}$$

$$Re_v = \frac{G_{flux} \cdot 7x \cdot d_{in}}{\mu_v} \tag{35}$$

$$Re_l = \frac{G (1 - 7x) \cdot d_{in}}{\mu_l} \tag{36}$$

5.3.3 Sub-Cooling Region

After leaving the two-phase region, sub-cooling zone begins with the condenser. ($\dot{Q}_{sub}$) sub-cooling concentrations can be determined:

$$\dot{Q}_{sub} = \alpha_{sub} \cdot A_{sub} \cdot \left(T_{med,out} - T_{trans,out} \right) \tag{37}$$

$$\alpha_{sub} = 0.023 \cdot Re_4^{0.8} \cdot Pr_4^{0.4} \cdot \frac{k_4}{d_{in}} \tag{38}$$

$$T_{med,out} = \frac{h_5 - h_4}{s_5 - s_4} \tag{39}$$

To find the total length of the HWC.

$$L_{total} = L_{single,phase} + \sum_{n=1}^{n=14} L_{tp} \tag{40}$$

$$L_{single,phase} = L_{sh,1} + L_{sh,2} + L_{sub} \tag{41}$$

$$\sum_{n=1}^{n=14} L_{tp} = \sum_{n=1}^{n=6} L_{tp,right} + \sum_{n=9}^{n=14} L_{tp,left} + \sum_{n=7}^{n=8} L_{tp,top} \tag{42}$$

A program was built in Engineering Equation Solver (EES) Software based on the previous MM. The below is a flow chart for the software.

5.4 Dimensional and Functional Parameter of the Condenser

NTC thermistor are used to read temperatures in several areas of the refrigerator.

5.5 Validation of the mathematical model
5.5.1 Validation with experimental results

The tables below show the data of refrigerants R600a, R134a, and R1234yf have been resulted from each experiment.

Table 5-1: The validation of t_5 for R600a.

t_amb ºC	p_cond / p_evap	n	t_c ºC	t_EES ºC	t_exp ºC	t_deviation %
22	13.98	1.046	51.95	38.95	46.95	2.49
23	14.1	1.045	53.85	40.95	48.65	2.39
24	13.8	1.045	53.45	41.95	46.95	1.56
25	14.25	1.045	54.35	42.75	49.15	1.98
26	13.87	1.043	55.25	43.75	48.75	1.55
27	14.89	1.046	54.55	43.45	47.35	1.21
28	14.21	1.044	55.55	44.45	48.05	1.12
29	14.6	1.044	55.35	44.25	48.15	1.21

When using the EES program for the sub-cooling region, it was discovered that the number of control volumes are reduced at ambient temperature 29 [ºC] compared to ambient temperature 22 [ºC].

The influences of ambient temp. on the condenser region length in the laboratory refrigerator is seen in Table 5.2.

Table 5-2: Ambient temperature effect on condenser pipe length.

t_amb [ºC]	L 1sh [m]	L tph [m]	L sub [m]	L_total [m] R600a	L 1sh [m]	L tph [m]	L sub [m]	L_total [m] R134a	L 1sh [m]	L tph [m]	L sub [m]	L_total [m] R1234yf
22	0.178	6.37	0.351	6.89	0.83	5.51	0.56	6.9	1	6.98	----	7.98
23	0.184	6.34	0.368	6.89	0.89	5.5	0.51	6.9	0.96	6.65	----	7.62
24	0.202	6.268	0.43	6.9	0.82	5.65	0.44	6.91	0.68	6.56	----	7.24
25	0.198	6.282	0.42	6.9	0.9	5.82	0.18	6.9	1.1	7.23	----	8.33
26	0.189	6.174	0.537	6.9	0.95	5.88	0.08	6.91	0.85	6.59	----	7.44
27	0.201	6.095	0.604	6.9	0.95	5.89	0.06	6.9	0.84	6.98	----	7.82
28	0.22	5.99	0.69	6.9	1.22	6.46	---	7.68	1.03	7.17	----	8.2
29	0.255	5.896	0.75	6.9	1.43	7.09	---	8.52	0.86	6.17	----	7.3

5.5.2 Validation with results published in the literatures

Another kind of validation is done to make sure that the model is applicable to different types of refrigerators. The first validation is with Espíndola et al. [44], and the second with Ghule and Mahajan [45].

6   Results

It is noted that the value of the power increases in each time the ambient temperature increases, which is greatly affected by the increase in the value of the ambient temperature.

Figure 6.1 shows the relationship between ambient temperature distribution and condensation pressure for R600a, R134a and R1234yf refrigerants.

Figure 6-1: Relation between ambient temperature and condenser pressure.

Figure 6.2 explains the behavior of the condenser sub-cooling length with the ambient temperature.
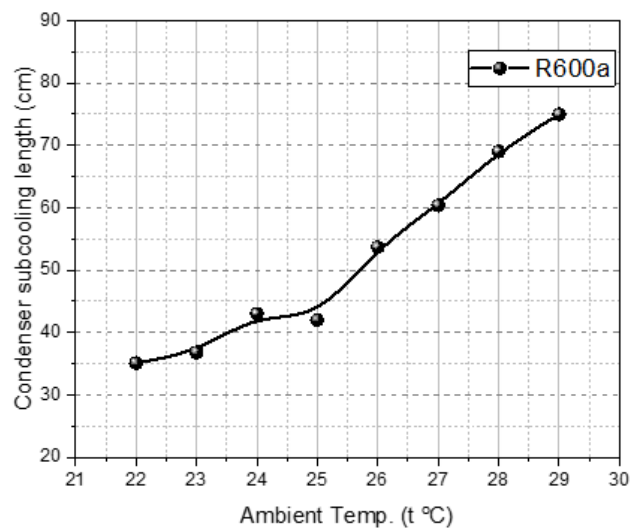
Figure 6-2: Condenser sub-cooling length and ambient temperature.

The (EES) software was used to compare the sub-cooling temperature T_5 to the refrigerant outlet temperature from the condenser, as shown in figure 6.3.

Figure 6.4 represented the relationship between ambient temperature distribution and condensation temperature for R600a, R134a and R1234yf refrigerants..
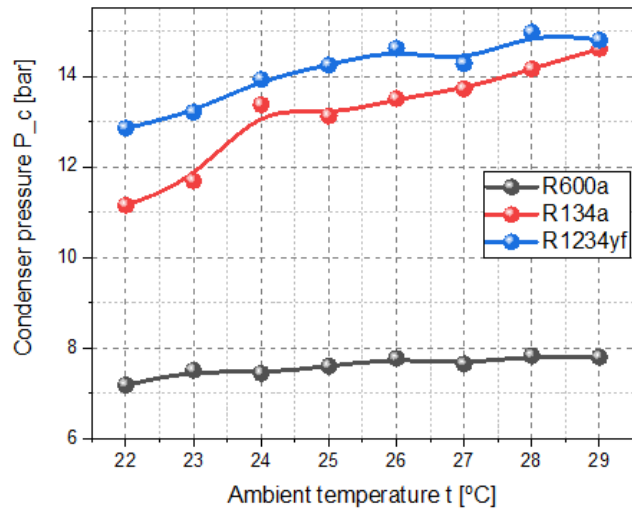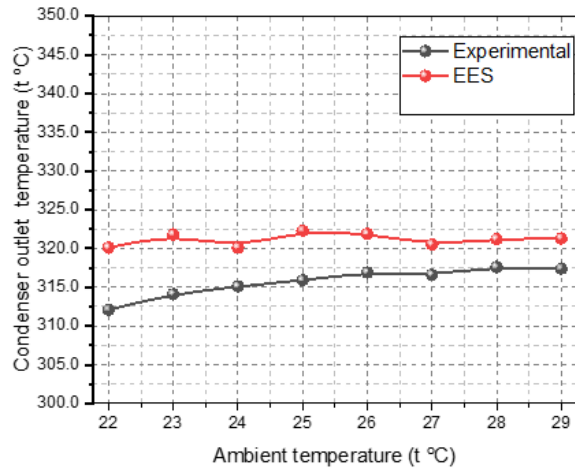
Figure 6-3: R600a Experiment and EES sub-cooling temperature t_5.
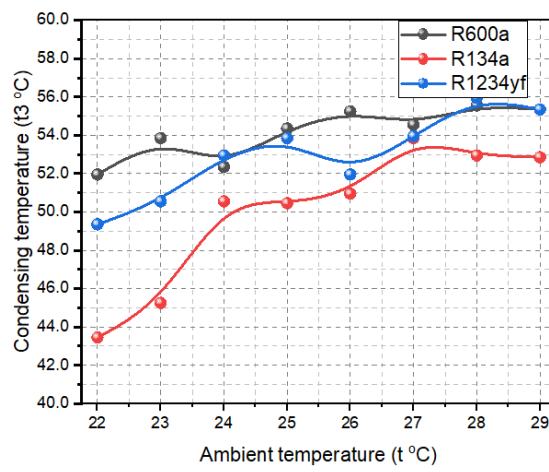
Figure 6-4: Condensing and ambient temperature.

7 Conclusions, Contributions, and Future Work

7.1 Conclusions

Some of the most important results from the tests are as follows:

- For a given compressor stroke, the $\dot{m}$ of R1234yf is higher than R134a and R600a.
- At a temperature of 29, the R1234yf $\dot{m}$ is 8.7% greater than R134a, while $\dot{m}$ is estimated to be around 57.7% higher than R600a
- The discharge temperature of R600a was shown to be 12 to 16 ºC lower than R134a and 7 to 16ºC lower than R1234yf.
- R600a's power consumption was determined to be 10.2–24.3% lower than R134a's and R1234yf's, respectively, by 22–26.9% and 22–26.9%.
- Because of higher friction, the evaporator pressure of R1234yf is higher than R134a and R600a for a given $\dot{m}$.
- In the case of HRC, the study proposes a simple MM that may be used to calculate the refrigerant $\dot{m}$.
- Practical experiments demonstrate that the specifications of R1234yf and R134a refrigerants are highly converging, particularly in terms of temperature, energy consumption, and $\dot{m}$. However, unless the VCR system is modified, none of the two refrigerants may be utilized to replace the R600a refrigerant.
- The internal temperatures of the shell, also referred to as the temperature of the capsule, and the muffler section, also referred to as the entry point to the compressor section inside the compressor, are compared in this compressor validation. Previous studies have indicated that the temperature inside the compressor approaches the same values as we calculated, especially for the refrigerants R600a or R134a.
- In the first section of the validation, a comparison between our work and that of Posch et al. is shown for the internal temperature of the shell, R600a, and 3000 rpm. t_{amb} = 32 ºC, $t_{muffler\ section}$ = 55 ºC, and t_{cond} = 45 ºC are the temperature limits. In contrast to 51.55 ºC for the previous study, the temperature of the interior (surface) of the shell as observed in our work is 57.8 ºC with a 1.9 % deviation (Posch et al., 2018) [46].
- Another area where our findings and that of Dutra et al. [161] are contrasted is the internal temperature of the shell, R134a. This shows how similar or dissimilar our work is to Dutra et al.'s. The compressor's interior temperature can frequently exceed 96 ºC, according to study. The results of comparing the work of Dutra et al. table 4-7 at t_{amb} = 32 ºC and the current study at t_{amb} = 29 ºC reveal that: $t_{shell\ inside}$ for Dutra et al. = 65-78 ºC at t_c = 54 ºC and $t_{shell\ inside}$ for 83-96 ºC at T_c = 90 ºC, while $t_{shell\ inside}$ for our work = 75.15 ºC at t_c = 71.52 ºC.
- For the second part of the validation, a comparison of our research and that of Ozdemir et al. [47] about the internal temperature of the muffler section is provided. It has been shown that the temperature of the muffler section in our investigation may be higher as a result of heat transmission between the mechanical parts and the electrical motor's activation. P_e (17.7%%), P_c (1.3%), t_c (8.4%), t_{amb} (9.4%), $t_{shell\ inside}$ (0.15%), and $t_{muffler\ section\ inlet}$ all had deviation rates higher than the comparative average (16.1%).

For the justifications for utilizing the HWC. The flowchart of the experiment's parameters was used to create a MM that was also presented.

- The validation predictions for T5 between the experimental results and the MM seems to be extremely accurate, with the total variances ranging from 1.43 to 2.49% at varied temperatures between 22 and 29 °C.
- The length of the portion of the super-heated area increases as ambient temperature increases.
- The condenser heat rejected from a HR was predicted to be affected by ambient temperature. Additionally, the results demonstrated that as R600a's ambient temperature increases, the sub-cooling region also increases.
- The super-heated condenser will get longer as the $\dot{m}$ rises.
- The length of the super-heated region will decrease when t 3r is increased.
- Due to the high degree of specification convergence, the R1234yf refrigerant may be utilized in replacement of the R134a refrigerant.
- A system that uses R600a refrigerant cannot be replaced with R134a or R1234yf.
- We performed a validation with the angle of contact of the insulation tape between foam and tube that insulates the tube surface from heat transfer to the refrigerator to increase our confidence in the accuracy of our work since research assumes that the angle (θ) is 95 percent to simplify calculations. Most studies discuss calculating the value of the angle (θ) theoretically, where the angle value was computed from the outside, as opposed to what we have done, which is to calculate the angle from the inside. When compared to Ghule and Mahajan's [45]. data on the proportion of tubes in contact with tape from the outside, our work's empirically estimated angle has a value of 72 percent, or with a deviation of about 2.8% [45]. The insulating tape reduces the interior angle of 100º to a 28 percent inside contact angle, which, when divided by 360 degrees, equals to a 72 % outside angle.
- Additional validation is done to show that the model is relevant to different types of refrigerators. The first validation was provided by Espndola et al. [48], while the second validation was provided by [45]. The data from the two investigations were replaced in our software with data that gave excellent outcomes for the length and diameter of the condenser, subcooling duration, and superheated, two-phase flow behavior.
- In the original experimental work, the refrigerator's dimensions were 160.6 cm in height, 62 cm in width, and 70 cm in length; in our work or model, they are 60×50×50 cm³. We employ the shape of the condenser, the type of R600a refrigerant, the diameter of the condenser, and the other unspecified boundary conditions from our study.
- Our software produced great results, notably in recognizing and locating superheated, two-phase flow, and sub-cooling zones because the condenser length is almost the same after running it. For superheated, 890 cm for two-phase flow, and 127 cm for subcooling, the lengths were roughly 70 cm. The sum of lengths is 1087 cm, which is 0.6 percent off from Espndola et al. measurements (1080 cm). Additionally, there was a 0.09 percent deviation between the temperature entering the capillary tube and exiting the condenser, which was 314.7 K in comparison to Espndola et al. investigation (41.85 ºC).
- We modified our EES method to use R134a as the kind of refrigerant in the second study (Ghule & Mahajan) [45], replacing the pressure, temperature, and $\dot{m}$. The entire length was 16.8 m, the $\dot{m}$ was 0.00047848 kg/s, the condenser pressure was 13.624 bar (Ghule

& Mahajan)[45]. Since the condenser length is so close, our program's results likewise produced great results. For superheated, 14.5 m for two-phase flow, and 0.9 m for sub-cooling, the lengths were roughly 1.21 m. The total lengths are 16.61 m with a 1.1 percent deviation compared to Ghule and Mahajan's work (16.8 m).

7.2 Contributions

This section will divide into two paragraphs, the first is the thesis outcomes and the second is originality.

7.2.1 Thesis outcomes

The main outcomes of the thesis are:

- The MM which can estimate the $\dot{m}$ of a given HRC operating with refrigerants R600a, R134a, and R1234yf for different ambient temperatures as mentioned in section 4.4

- The MM which can simulate the operation of a given HWC working with refrigerants R600a, R134a, and R1234yf for different ambient temperatures as mentioned in section 5.3. The MM divides the HWC into de-superheating, condensing, and subcooling regions. Also, upward and downward flow paths are used. The MM can be used or extended as a design tool for new HWC operating in totally different conditions. This can be a very useful tool for companies activating in the field of HR manufacturing because it can avoid the trial-and-error process.

- an experimental setup based on a small HR instrumented to validate the theoretical results obtained with the MM developed in the present work as mentioned in section 3.1.

- The HRC customized for the presented thesis having sensors mounted inside the shell. Using the sensors, the operation of the HRC can be studied in different ambient conditions for refrigerants R600a, R134a, and R1234yf as mentioned in section 3.3.

- a database containing experimental data describing the operation of the HRC as in section 4.5.1, and the HWC mounted on such small HR as presented in section 5.4.1. The experimental data available in literature dealing with the subject of the Theis are rather few, compared to other research fields.

The interior angle of the connecting pipe with the refrigerator side wall was calculated by 100º, and after dividing it by 360 degrees, it becomes a 28º inside contact angle with the insulating tape, which is approximately 72º outside angle

7.2.2 Original contributions

The original contributions are summarized below.

Using the HRC customized for the presented thesis, valuable information regarding the temperature of refrigerants R600a, R134a, and R1234yf at the compressor suction port has been obtained. High superheating degrees have been noticed for the studied refrigerants as mentioned in section 5.4.1. This is an indicator that the HRC mounted on such small HR operates in difficult conditions. Similar results have been indicated in the literature for other test conditions as presented in section 4.6.2, table 4-7. Also, the experimental data available in the literature is rather small in this case.

Using the HWC model, the operation of such heat exchangers can be evaluated in different ambient temperatures and different refrigerants. The most important results indicate that:

- at the same ambient temperature of 22 to 29 ºC, the length of the de-superheating zone in the case of R600a is 17.8 to 25.5 cm. The length of the super-heated area for refrigerant R134a and refrigerant R1234yf reached 83 cm and 100 cm, at the ambient temperature of 22 ºC, while at the ambient temperature of 29 ºC, the super-heated length reached 143 cm and 86 cm for R134a and R1234yf, respectively as shown in table 5-9.

- at the same ambient temperature, the length of the two-phase zone in the case of R600a is 6.37 to 5.89 m. The length of two-phase length for refrigerant R134a and refrigerant R1234yf reached 5.5 m and 6.9 m, at the ambient temperature of 22 ºC, while at the ambient temperature of 29 ºC, the two-phase length reached 7 m and 6.1 m for R134a and R1234yf, respectively as presented in table 5-9.

- as the ambient temperature increases the length of the two-phase zone is decreasing while the length of the subcooling and de-superheating zone increases. Also, the length of the de-superheating zone generally displays higher values than the subcooling zone as in the table 5-9.

Data available in literature has been inserted in the presented MM for the HWC and the obtained results are in good agreement with similar work conducted as shown in section 5.5.1.

The contact angle θ between the aluminum foil and the HWC pipes has been estimated empirically as in figures 5-4 and 5-5. The result obtained is in good agreement with other reported data as presented in section 5.3.1.2.

7.3 Future Work

- Manufacturing the condenser tube in an oval shape is recommended to study the system performance, and how the shape can affected on heat transfer.
- Changing the compressor type from reciprocating to variable speed to study the impact of changing the speed on the system performance.

References

[1]   S. Bista, S. E. Hosseini, E. Owens, and G. Phillips, "Performance improvement and energy consumption reduction in refrigeration systems using phase change material (PCM)," *Appl Therm Eng*, vol. 142, pp. 723–735, Sep. 2018, doi: 10.1016/j.applthermaleng.2018.07.068.

[2]   J. al Douri *et al.*, "Preliminary experimental assessment of a vertical shell and tube heat exchanger based on phase change materials," *IOP Conf Ser Mater Sci Eng*, vol. 1262, no. 1, p. 012077, Oct. 2022, doi: 10.1088/1757-899x/1262/1/012077.

[3]   S. Choi, U. Han, H. Cho, and H. Lee, "Review: Recent advances in household refrigerator cycle technologies," *Applied Thermal Engineering*, vol. 132. Elsevier Ltd, pp. 560–574, Mar. 05, 2018. doi: 10.1016/j.applthermaleng.2017.12.133.

[4]   C. IONITA, E. E. VASILESCU, L. POPA, H. POP, S. J. S. ALQAISY, and I. UTA, "EXERGY ANALYSIS OF LIQUID AIR ENERGY STORAGE SYSTEM BASED ON LINDE CYCLE," *INMATEH Agricultural Engineering*, pp. 543–552, Aug. 2022, doi: 10.35633/inmateh-67-53.

[5]   G. F. Hundy, A. R. Trott, and T. C. Welch, *Refrigeration and Air Conditioning*, Fourth Edi. United Kingdom, 2010.

[6]   C. P. Arora, *Refrigeration-and-air-conditioning*, Second edi. India: Tata McGraw-Hill, 2006.

[7]   J. al Douri, K. S. Hmood, V. Apostol, H. Pop, S. J. Alqaisy, and E. Beatrice Ibrean, "Review regarding defrosting methods for refrigeration and heat pump systems," *E3S Web of Conferences*, vol. 286, p. 01012, 2021, doi: 10.1051/e3sconf/202128601012.

[8]   E. Navarro, J. F. Urchueguıa, J. M. Corberan, and E. Granryd, "Performance analysis of a series of hermetic reciprocating compressors working with R290 (propane) and R407C," *International Journal of Refrigeration*, vol. 30, pp. 1244–1253, 2007, doi: 10.1016/j.irefrig.2007.02.006.

[9]   D. K. Ramesha, S. Kiran, and K. Kushal, "An Overview of Propane Based Domestic Refrigeration Systems," *Materials Today*, vol. 5, pp. 1599–1606, 2018.

[10]   Y. A. ÇENGEL, M. A. BOLES, and M. KANOĞLU, *Thermodynamics An Engineering Approach*, Ninth Edit. New York, USA: McGraw-Hill Education, 2019.

[11]   C. D. Peʹrez-Segarra, J. Rigola, M. Soʹria, and A. Oliva, "Detailed thermodynamic characterization of hermetic reciprocating compressors," *International Journal of Refrigeration*, vol. 28, pp. 579–593, 2005, doi: 10.1016/j.ijrefrig.2004.09.014.

[12]   D. Ndiaye and M. Bernier, "Dynamic model of a hermetic reciprocating compressor in on – off cycling operation (Abbreviation : Compressor dynamic model)," *Appl Therm Eng*, vol. 30, no. 8–9, pp. 792–799, 2010, doi: 10.1016/j.applthermaleng.2009.12.007.

[13]   M. K. Ibrahim Dincer, *Refrigeration Systems and Applications*, Second Edi. United Kingdom: A John Wiley and Sons, Ltd., Publication, 2010.

[14]   A. E. Gürel, Ü. Ağbulut, A. Ergün, and İ. Ceylan, "Environmental and economic assessment of a low energy consumption household refrigerator," *Engineering Science and Technology , an International Journal*, no. xxxx, 2019, doi: 10.1016/j.jestch.2019.06.003.

[15]   H. Jin *et al.*, "A detrending-extracting-zooming-based speed measurement method for hermetic reciprocating compressor," *Measurement*, vol. 157, p. 107654, 2020, doi: 10.1016/j.measurement.2020.107654.

[16]   A. Y. Faraji, H. J. Goldsmid, and A. Akbarzadeh, "Experimental study of a thermoelectrically-driven liquid chiller in terms of COP and cooling down period," *Energy Convers Manag*, vol. 77, pp. 340–348, 2014, doi: 10.1016/j.enconman.2013.09.047.

[17]   P. Bansal, E. Vineyard, and O. Abdelaziz, "Advances in household appliances- A review," *Appl Therm Eng*, vol. 31, no. 17–18, pp. 3748–3760, 2011, doi: 10.1016/j.applthermaleng.2011.07.023.

[18]   R. Zhou *et al.*, "Heat Transfer Simulation for Reciprocating Compressor with Experimental Validation," in *10th International Conference on Compressors and their Systems, Materials Science and Engineering Volume 232*, 2017. doi: 10.1088/1757-899X/232/1/012011.

[19] A. R. Ozdemir, E. Oguz, and S. Onbasioglu, "An investigation of the heat transfer phenomena between the hermetic reciprocating compressor components," in *8th International Conference on Compressors and their Systems*, 2013, pp. 385–395. doi: 10.1533/9781782421696.7.385.

[20] Shailesh Golabhanvi and V. Navadagi, "Thermal and Performance Analysis of R600a in Vapour Compression Cycle," *International Journal of Engineering Research and*, vol. V7, no. 01, pp. 35–40, 2018, doi: 10.17577/ijertv7is010024.

[21] T. S. Pilla, P. K. G. Sunkari, S. L. Padmanabhuni, S. S. Nair, and R. S. Dondapati, "Experimental Evaluation Mechanical Performance of the Compressor with Mixed Refrigerants R-290 and R-600a," *Energy Procedia*, vol. 109, pp. 113–121, 2017, doi: 10.1016/j.egypro.2017.03.065.

[22] N. Zhang, B. Li, L. Feng, and Y. Dai, "Research on the Thermophysical Properties and Cycle Performances of R1234yf/R290 and R1234yf/R600a," *Int J Thermophys*, vol. 42, no. 8, pp. 1–22, 2021, doi: 10.1007/s10765-021-02875-0.

[23] S. Bobbo, R. Stryjek, N. Elvassore, and A. Bertucco, "A recirculation apparatus for vapor-liquid equilibrium measurements of refrigerants. Binary mixtures of R600a, R134a and R236fa," *Fluid Phase Equilib*, vol. 150, no. 151, pp. 343–352, 1998, doi: 10.1016/s0378-3812(98)00334-3.

[24] M. M. Joybari, M. S. Hatamipour, A. Rahimi, and F. G. Modarres, "Exergy analysis and optimization of R600a as a replacement of R134a in a domestic refrigerator system," *International Journal of Refrigeration*, vol. 36, no. 4, pp. 1233–1242, 2013, doi: 10.1016/j.ijrefrig.2013.02.012.

[25] P. Reasor, V. Aute, and R. Radermacher, "Refrigerant R1234yf Performance Comparison Investigation," in *International Refrigeration and Air Conditioning Conference at Purdue*, 2010, pp. 1–7.

[26] T. Kamiaka, C. Dang, and E. Hihara, "Vapor-liquid equilibrium measurements for binary mixtures of R1234yf with R32, R125, and R134a," *International Journal of Refrigeration*, vol. 36, no. 3, pp. 965–971, 2013, doi: 10.1016/j.ijrefrig.2012.08.016.

[27] Z. Li, K. Liang, and H. Jiang, "Experimental study of R1234yf as a drop-in replacement for R134a in an oil-free refrigeration system," *Appl Therm Eng*, vol. 153, no. March, pp. 646–654, 2019, doi: 10.1016/j.applthermaleng.2019.03.050.

[28] M. Mohanraj, S. Jayaraj, C. Muraleedharan, and P. Chandrasekar, "Experimental investigation of R290/R600a mixture as an alternative to R134a in a domestic refrigerator," *International Journal of Thermal Sciences*, vol. 48, no. 5, pp. 1036–1042, 2009, doi: 10.1016/j.ijthermalsci.2008.08.001.

[29] P. Lu, S. Deng, B. Yang, and L. Zhao, "Numerical simulation on constituents separation of R134a/R600a in a horizontal T-junction," *International Journal of Refrigeration*, vol. 115, pp. 148–157, 2020, doi: 10.1016/j.ijrefrig.2020.03.006.

[30] V. A. Rykov, S. V. Rykov, and A. V. Sverdlov, "Fundamental equation of state for R1234yf," *J Phys Conf Ser*, vol. 1385, no. 1, 2019, doi: 10.1088/1742-6596/1385/1/012013.

[31] J. Hu, L. Yang, L. L. Shao, and C. L. Zhang, "Generic network modeling of reciprocating compressors," *Energy Econ*, vol. 45, pp. 107–119, 2014, doi: 10.1016/j.ijrefrig.2014.06.007.

[32] K. S. Hmood, H. Pop, V. Apostol, S. al Qaisy, and V. Badescu, "Steady-state performance of capillary tubes for small-scale vapour compression systems using different refrigerants," *International Journal of Refrigeration*, vol. 130, pp. 87–98, Oct. 2021, doi: 10.1016/j.ijrefrig.2021.06.015.

[33] H. Pop, V. Apostol, S. J. Alqaisy, K. S. Hmood, J. al Douri, and V. Badescu, "mass flow rate evaluation of a hermetic compressor from a small scale vapour compression refrigeration system," *U.P.B. Sci. Bull., Series D*, vol. 83, no. 1, p. 2021.

[34] W. Li, "Simplified steady-state modeling for hermetic compressors with focus on extrapolation.," *International Journal of Refrigeration*, vol. 35, no. 6, pp. 1722–1733, 2012, doi: 10.1016/j.ijrefrig.2012.03.008.